

# Novel size effects on magneto-optics in the spherical quantum dots

Manvir S. Kushwaha

We embark on investigating the magneto-optical absorption in *spherical* quantum dots *completely* confined by a harmonic potential and exposed to an applied magnetic field in the symmetric gauge. This is done within the framework of Bohm-Pines' RPA that enables us to derive and discuss the full Dyson equation that takes proper account of the Coulomb interactions. Intensifying the confinement or magnetic field and reducing the dot-size yields a blue-shift in the absorption peaks. However, the size effects are seen to be predominant in this role. The magnetic field tends to maximize the localization of the particle, but leaves the peak position of the radial distribution intact. The intra-Landau level transitions are forbidden.

**Introduction:** The scientific quest behind the synthesis of semiconducting quantum dots is to create and control future electronic and optical nanostructures, which are quantally engineered by tailoring the shape, size, and composition. Scientists have approached the fabrication of quantum dots – the ultimate in quantum confinement – from two very different points of view: (i) a top-down approach in which the extent and dimensionality of the solid has gradually been reduced, and (ii) a bottom-up in which quantum dots are viewed as extremely large molecules or colloids. The quantum dots grown by epitaxial and lithographic techniques are in the size regime from 1  $\mu\text{m}$  down to 10 nm, whereas the colloidal samples vary in diameter from the truly molecular regime of 1 nm to about 20 nm. The latter systems are also known in the literature by the names of colloidal quantum dots or nanocrystals: The spherical quantum dots (SQDs) are the precise examples of this family playing better responsive role as lasers than their epitaxial-cum-lithographic counterparts [1].

The research interest burgeoned in SQDs has focused largely on the exciton dynamics of the bulk part with the surface states, generally, eliminated by enclosure in a material of larger band-gap [2-7]. As such, the scrutiny of the existing literature on the SQDs reveals the lack of genuine efforts devoted to theorizing the magneto-optical absorption that rigorously justifies the (localized) plasmon excitation peaks observed in the optical experiments. The present letter is motivated to fill that gap.

**Theoretical framework:** We consider a quasi-zero dimensional electron system (Q0DES) three-dimensionally confined by a harmonic potential  $V(\mathbf{r}) = \frac{1}{2} m^* \omega_o^2 r^2$  and subjected to an applied magnetic field in the symmetric gauge [ $\mathbf{A}(\mathbf{r}) = \frac{1}{2} (\mathbf{B} \times \mathbf{r})$ ] in the spherical geometry [with  $\mathbf{r} \equiv (r, \theta, \phi)$ ]. For such a typical Q0DES, the single-particle [of charge  $-e$ , with  $e > 0$ ] Hamiltonian in the Coulomb gauge [ $\nabla \cdot \mathbf{A} = 0 \Rightarrow \mathbf{A} \cdot \mathbf{p} = \mathbf{p} \cdot \mathbf{A}$ ] can be expressed as

$$H = -\frac{\hbar^2}{2m^*} \nabla^2 + \frac{1}{2} \frac{eB}{m^*c} \hat{L}_z + \frac{1}{8} \frac{e^2}{m^*c^2} (\mathbf{B} \times \mathbf{r})^2 + \frac{1}{2} m^* \omega_o^2 r^2, \quad (1)$$

where  $c$ ,  $m^*$ ,  $\mathbf{p}$ ,  $\mathbf{A}$ ,  $\mathbf{B}$ , and  $\omega_o$  are, respectively, the speed of light in the vacuum, electron effective mass, momentum operator, vector potential, magnetic field, and the characteristic frequency of the harmonic oscillator. The operator  $\hat{L}_z = -i\hbar \frac{\partial}{\partial \phi}$  is the z-component of the angular momentum. The harmonic potential confining the SQDs is the most reasonable choice justifiable for the situation with small number of electrons ( $N$ ) in the dots. This model potential validates the generalized Kohn theorem (GKT) [8], which states that the FIR resonant spectrum of a correlated many-electron system is insensitive to the interaction effects. Obviously, we consider a one-component plasma inside the Q0DES and neglect the spin-orbit interactions and the Zeeman energy for the sake of simplicity. Making use of the Laplacian operator  $\nabla^2$  (in the spherical coordinates), substituting  $\Psi(r, \theta, \phi) = R(r)\Theta(\theta)\Phi(\phi)$ , and transposing allows us to solve the Schrodinger equation  $H\Psi = \epsilon\Psi$ ; with  $\epsilon$  being the eigenenergy. The result is that the Q0DES can be characterized by the eigenfunction  $\Psi(r, \theta, \phi) = R_{nl}(r) Y_l^m(\theta, \phi)$ , where the radial function

$$R_{nl}(r) = N_r e^{-X/2} X^{l/2} \Phi(-\alpha_{nl}; 1 + S; X), \quad (2)$$

where  $S = \frac{1}{2} + l$ ,  $X = r^2/l_H^2$ , and  $N_r$  is the normalization coefficient. Here  $X = |r|_{r=R}$ , and  $\Phi(-\alpha_{nl}; 1 + S; X)$ ,  $l_H = \sqrt{\hbar/(m^* \Omega_H)}$ ,  $\Omega_H = \sqrt{\frac{\omega_o^2}{4} \sigma^2 + \omega_o^2}$ ,  $\omega_c = eB/(m^*c)$ , and  $R$  are, respectively, the confluent hypergeometric function (CHF), the hybrid magnetic length, the hybrid

characteristic frequency, the cyclotron frequency, and the dot radius; and the spherical harmonics are defined as

$$Y_l^m(\theta, \phi) = N_y P_l^m(\cos \theta) e^{im\phi}, \quad (3)$$

where  $P_l^m(\cos \theta)$  is the associated Legendre function and  $N_y$  is the normalization coefficient. Here  $n$ ,  $l$ , and  $m$  are, respectively, the principal, orbital, and magnetic quantum numbers. The spherical harmonics satisfy the well-known condition of orthonormality. The finiteness of the quantum dot requires that the eigenfunction  $\Psi(\dots)$  satisfies the boundary condition  $R_{nl}(r=R) = 0 \Rightarrow \Phi(-\alpha_{nl}; 1 + S; X) = 0$ . This determines the eigenenergy of the system defined by

$$\epsilon_{nlm} = 2\hbar\Omega_H \left[ \alpha_{nl} + \frac{1}{2} (1 + S) \right] + \frac{1}{2} m \hbar \omega_c \quad (4)$$

In this form, the eigenenergy for SQDs is *formally* identical to that for the quantum dots laterally confined in the Q2DES [1]. It is important to notice the appearance of the symbol  $\sigma$  defined by  $\sigma^2 = \langle l'm' | \sin^2 \theta | lm \rangle$  in the definition of  $\Omega_H$ . In order to investigate the magneto-optical absorption in the semiconducting SQDs, what we actually need to compute sagaciously is only the energy dependence of the *imaginary* part of the interacting (or total) density-density correlation function (DDCF)  $\chi(\dots)$ , where

$$\begin{aligned} \chi(\omega) &= \int d\mathbf{r} \int d\mathbf{r}' \chi(\mathbf{r}, \mathbf{r}'; \omega) \\ &= \sum_{ijkl} [\Pi_{ij} \delta_{ik} \delta_{jl} + \Pi_{ij} \sum_{mn} \Lambda_{klmn} \Pi_{mn} F_{mnij}] \\ &\quad \times \int d\mathbf{r} \int d\mathbf{r}' \Psi_i^*(\mathbf{r}) \Psi_j(\mathbf{r}) \Psi_l^*(\mathbf{r}') \Psi_k(\mathbf{r}'), \end{aligned} \quad (5)$$

where  $\Pi_{ij} = [f(\epsilon_i) - f(\epsilon_j)]/[\epsilon_i - \epsilon_j + \hbar\omega + i0^+]$ ,  $\Lambda_{\mu\nu}$  is the inverse of  $[\delta_{\mu\nu} - \Pi_{\mu}\beta_{\mu\nu}]$  such that  $\sum_{\mu} \Lambda_{\gamma\mu} [\delta_{\mu\nu} - \Pi_{\mu}\beta_{\mu\nu}] = \delta_{\gamma\nu}$ , and  $F_{mnij} = \int d\mathbf{r}'' \int d\mathbf{r}''' \Psi_m^*(\mathbf{r}'') \Psi_n(\mathbf{r}'') V_{ee}(\mathbf{r}'', \mathbf{r}''') \Psi_j^*(\mathbf{r}''') \Psi_i(\mathbf{r}''')$  stands for the matrix elements of the Coulombic interaction potential  $V_{ee}(\mathbf{r}, \mathbf{r}')$ . Here  $f(\epsilon_j)$  is the Fermi-Dirac distribution function, and  $\beta_{\mu\nu} = \int d\mathbf{r} L_{\mu}^*(\mathbf{r}) S_{\nu}(\mathbf{r})$ ; with the symbols  $L_{\mu}(\mathbf{r})$  and  $S_{\mu}(\mathbf{r})$  representing, respectively, the long-range and the short-range parts of the Coulombic interactions discussed in the strategy leading to the determination of the inverse dielectric function  $\epsilon^{-1}(\mathbf{r}, \mathbf{r}'; \omega)$  [1] and the subscript  $\mu, \nu \equiv i, j$  is a composite index introduced just for the sake of the mathematical convenience. Equation (5) is a variant of the Dyson equation derived within the framework of the Bohm-Pines' full RPA [1].

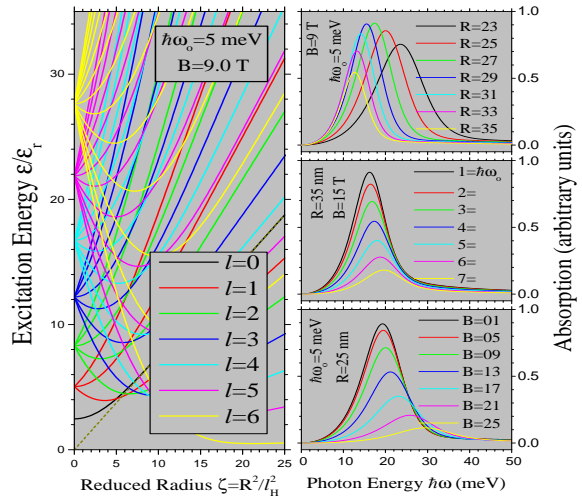


**Fig. 1** (Color online) Left panel: The Fock-Darwin excitation spectrum for the GaAs SQDs in the presence of an applied magnetic field ( $B$ ), for several values of  $l \leq 6$ . The dashed line represents the lowest branch of the magnetic (or Landau) fan – when  $\alpha_{nl} \rightarrow 0$  for very large  $R$  or  $B$ . We chose not to plot the whole magnetic fan in order to avoid the mess.

**Fig. 2** (Color online) Right panel: The magneto-optical absorption vs. the excitation energy for the GaAs SQDs for several values of the dot radius  $R$  [top panel], confinement potential  $\hbar\omega_o$  [middle panel], and magnetic field  $B$  [bottom panel]. Other parameters are listed inside.

**Results and Discussion:** We focus on colloiddally prepared GaAs SQDs, which implies that the background dielectric constant  $\epsilon_o = 12.8$  and  $m^* = 0.067 m_o$ ; with  $m_o$  as the bare electron mass. The other parameters involved in the computation are:  $R$ ,  $\hbar\omega_o$ , and  $B$ . Until and unless stated otherwise, we specify the quantum numbers such that the dot contains (in total) 24 electrons (including spin). Also, we assume compliance of the lowest subband approximation due to harmonic confinement, which makes sense for the dots with small charge densities at low temperatures where most of the experiments are performed on the low-dimensional systems.

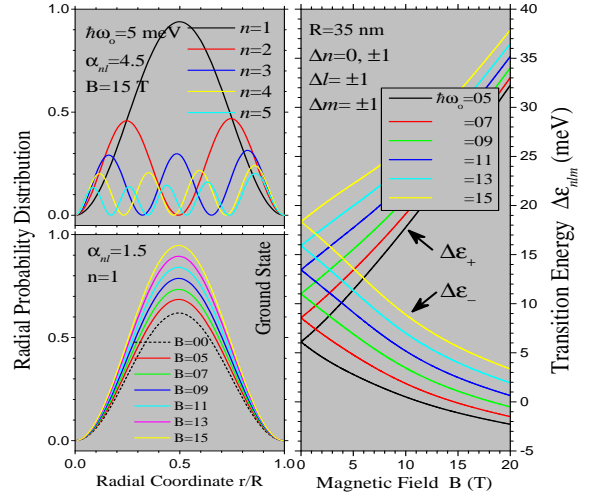
Figure 1 represents the Fock-Darwin excitation spectrum for the spherical quantum dot in the presence of a confinement potential ( $\hbar\omega_o = 5$  meV) and an applied magnetic field ( $B = 9$  T) for the orbital quantum number  $l \leq 6$ . The plots are rendered in terms of the dimensionless energy  $\epsilon_{nlm}/\epsilon_r$  and the dot radius  $\zeta = R^2/l_H^2$ ; with  $\epsilon_r = 2\hbar^2/(m^* R^2)$ . First and foremost, we observe that, unlike the laterally confined 2D quantum dots [1], the electronic levels at the origin are not equispaced. The  $(2l+1)$ -degeneracy at the origin justifies the intuition. All the modes with  $m \geq 0$  are seen to start and propagate throughout with a positive group velocity, whereas those with  $m < 0$  start with a negative group velocity, attain a minimum as  $\zeta$  increases, and finally propagate with the positive group velocity. The larger the  $|m|$ , the greater the value of  $\zeta$  where the latter type of modes observe a minimum. The dashed line starting from zero and finally merging with ( $l=0=m$ ) mode is the lowest branch of the magnetic fan. At large values of  $B$ ,  $\zeta$  becomes large, the role of  $\alpha_{nl}$  diminishes, and the magnetic fan is born.

Figure 2 illustrates the magneto-optical absorption as a function of the excitation energy for several values of the dot radius [top panel], confinement potential  $\hbar\omega_o$  [middle panel], and magnetic field  $B$  [bottom panel]. It is observed that the absorption peak experiences a blue shift as the confinement potential increases, the dot radius decreases, and the magnetic field increases. For example, by decreasing the radius from  $R = 35$  nm to  $R = 23$  nm, the peak position has blue-shifted by 31%. Similarly, increasing the confinement from  $\hbar\omega_o = 1$  meV to  $\hbar\omega_o = 7$  meV results in the peak position blue-shifted by 21%. Again, increasing the magnetic field from  $B = 1$  T to  $B = 25$  T yields a peak position blue-shifted by 52%. To sum up, reducing the dot-size and intensifying the confinement or the magnetic field enhances the capacity of the quantum dots to absorb the photons of higher energy. Also, the FWHM of the absorption peak increases with decreasing dot size and with increasing confinement or magnetic field. This reflects the tendency of the oscillator strength focused into a fewer transitions for the stronger confinement. By and large, the size effects predominate over those due to confinement or magnetic field.

Figure 3 shows the radial probability distribution (RPD) in the ground state against the (reduced) radial coordinate  $r/R$ . The RPD  $Q_{nl}(r)$  defined as  $Q_{nl}(r) = \int_0^\pi d\theta \sin\theta \int_0^{2\pi} d\phi r^2 |\Psi(r, \theta, \phi)|^2$  expresses the probability of finding an electron as a function of  $r$  at a given instant. The upper panel plots the ground states ( $l=0=m$ ) along with  $n=1, 2, 3, 4$ , and 5 for the magnetic field  $B = 15$  T. In the language of the spectroscopy, the principal quantum number  $n$  distinguishes the  $s$  orbitals – characterized by  $l=0$ . The lower panel of Fig. 3 exhibits the RPD in the ground state for several values of  $B$  in the range  $0 \leq B(T) \leq 15$ . Note that  $Q_{nl}(r)$  is zero at  $r=0$  because the volume of space available  $r^2 dr = 0$ . As  $r$  increases, the dot size increases and so does  $Q_{nl}(r)$ . However, the probability density  $|\Psi(r, \theta, \phi)|^2$  decreases with increasing  $r$ , which implies that the  $Q_{nl}(r)$ -path must have observed a maximum, where the probability of locating the electron is eminent. The influence of  $B$  on the variation of  $Q_{nl}(r)$  is remarkable: while the magnetic field tends to further add to the confinement and hence maximize the probability distribution with increasing  $B$ , it does not shift the peak position of the radial distribution, which lies at  $r/R \simeq 0.495$  for the whole range of  $B$ , including  $B=0$ .

Figure 4 describes the magneto-optical transitions in the spherical quantum dots as a function of magnetic field for a given value of the dot size ( $R = 35$  nm), for several values of the confinement potential ( $0.5 \leq \hbar\omega_o$  (meV)  $\leq 15$ ). Figure 4 is based on the computation of the exact analytical expression for the transition energy:  $\Delta\epsilon = 2[\Delta\alpha \pm \frac{1}{2}] \hbar\omega_H \pm \frac{1}{2} \hbar\omega_c$ ; where  $\Delta\alpha \equiv \Delta\alpha_{nl} = [\alpha_{1,1} - \alpha_{1,0}]$ . Some simple mathematical manipulations of this expression reveal that, unlike the laterally confined quantum dots [1], both – upper  $[\Delta\epsilon_+]$  and lower  $[\Delta\epsilon_-]$  – transitions survive whether or not  $\hbar\omega_o = 0$ . Similarly, at  $B=0$ , we obtain two, albeit relatively weaker, transitions given by  $\Delta\epsilon_{\pm} = 2[\Delta\alpha \pm \frac{1}{2}] \hbar\omega_o$ . Even when  $B \rightarrow \infty$  [i.e.,  $\omega_c \gg \omega_o$ ], we cannot avoid either of the two transitions. In other words, the SQDs do not allow the intra-Landau level transitions. Moreover, the non-zero parameters  $\sigma$  and  $\alpha_{nl}$  prevent the edges of the wedges to be exactly characterized by the confinement potential

( $\hbar\omega_o$ ) at  $B=0$ . These findings should prompt interesting magneto-optical experiments on the SQDs aimed at verifying such predictions.



**Fig. 3** (Color online) Left panel: The radial probability distribution  $Q_{nl}(r)$  in the ground state for the GaAs SQDs against the reduced (radial) coordinate  $r/R$ , for several values of  $n$ , which distinguishes the  $s$  orbitals characterized by  $l=0$ . The number of nodes equals  $(n-1)$ . The lower panel shows  $Q_{nl}(r)$  in the ground state ( $n=1, l=0, m=0$ ) for several values of  $B$ .

**Fig. 4** (Color online) Right panel: Allowed magneto-optical transitions vs. the magnetic field ( $B$ ), for several values of the confinement potential  $\hbar\omega_o$ . The dot radius is defined as  $R = 35$  nm. The selection rules are listed in the picture. The upper (lower) transition is designated as  $\Delta\epsilon_+$  ( $\Delta\epsilon_-$ ).

**Concluding remarks:** The magneto-optical absorption peak is blue-shifted with reducing dot-size and intensifying confinement or magnetic field. However, the size effects are observed to be predominant. While the magnetic field tends to maximize the probability of finding the electron, it does not shift the peak position of the RPD. Both – upper and lower – magneto-optical transitions survive even in the extreme cases of vanishing confinement or magnetic field. A deeper grasp of the importance of the spherical geometry [9] and of related aspects such as the quantum coherence, Coulomb blockade, and entanglement may lead to a better insight into the promising applications involving lasers, detectors, storage devices, and quantum computing, to name a few.

**Acknowledgment:** Sincere thanks to Loren Pfeiffer, Daniel Gammon, and Aron Pinczuk for the useful communication.

Manvir S. Kushwaha (Rice University, P.O. Box 1892, Houston, TX 77251)

E-mail: manvir@rice.edu

## References

- For an extensive review of electronic, optical, and transport phenomena in the systems of reduced dimensions such as quantum wells, quantum wires, and quantum dots, see M.S. Kushwaha, 'Plasmons and magnetoplasmons in semiconductor heterostructures', Surf. Sci. Rep., 2001, **41**, pp. 1-416
- A.L. Efros and A.L. Efros, 'Interband absorption of light in a semiconductor sphere', Sov. Phys.: Semiconductors, 1982, **16**, pp. 772-775
- L.E. Brus, 'Electron-electron and electron-hole interactions in small semiconductor crystallites: The size dependence of the lowest excited electronic state', J. Chem. Phys., 1984, **80**, pp. 4403-4409
- L. Banyai and S.W. Koch, 'Absorption blue shift in laser-excited semiconductor microspheres', Phys. Rev. Lett., 1986, **57**, pp. 2722-2724
- M.L. Steigerwald and L.E. Brus, 'Synthesis, stabilization, and electronic structure of quantum semiconductor nanocrystals', Annu. Rev. Mater. Sci., 1989, **19**, pp. 471-495
- Y. Wang and N. Herron, 'Nanometer-sized semiconductor clusters: Materials synthesis, quantum size Effects, and photophysical properties', J. Phys. Chem., 1991, **95**, pp. 525-532
- A.P. Alivisatos, 'Semiconductor clusters, nanocrystals, and quantum dots', Science, 1996, **271**, pp. 933-937
- F. M. Peeters, 'Magneto-optics in parabolic quantum dots', Phys. Rev. B, 1990, **42**, pp. 1486-1487
- J.K. Jain, *Composite Fermions* (Cambridge, New York, 2007).